

**Polarized front-illumination response in intraband quantum dot infrared photodetectors at 77 K**

E. Finkman,\* S. Maimon, V. Immer, and G. Bahir

*Department of Electrical Engineering and Solid State Institute, Technion, Haifa 32000, Israel*

S. E. Schacham

*Department of Electrical and Electronic Engineering, College of Judea and Samaria, Ariel 44837, Israel*

F. Fossard and F. H. Julien

*Institut d'Electronique Fondamentale, UMR 8622 CNRS, Univervite Paris-XI, 91405 Orsay, France*

J. Brault and M. Gendry

*Laboratoire d'Electronique-LEOM, UMR CNRS 5512, Ecole Centrale de Lyon, 69131 Ecully, France*

(Received 30 March 2000; revised manuscript received 26 June 2000; published 9 January 2001)

Multicolor quantum dot infrared photodetectors with normal incidence background limited performance (BLIP) at 77 K were implemented. The devices are composed of self-assembled InAs dots grown on InAlAs barrier layers, lattice matched to InP substrate. These dots are formed in a shape of flattened parallelepipeds. The photoconductive spectra were observed at all polarizations. Normal incidence photocurrent spectra reveal several polarized peaks in the range of 100–400 meV due to intersubband transitions. The detector responsivity at normal incidence is similar to that obtained for polarization normal to the layers, and is comparable to that achieved in quantum well infrared photodetectors (QWIP's). The transition energies, the polarization selection rules, and relative intensities of the peaks were tentatively interpreted in terms of a three-dimensional separation of variables.

DOI: 10.1103/PhysRevB.63.045323

PACS number(s): 73.21.-b, 78.66.Fd, 72.40.+w, 85.60.Gz

**I. INTRODUCTION**

It is exactly 200 years since the discovery of infrared radiation by Herschel.<sup>1</sup> All the important applications of infrared techniques (sciences, meteorology, medicine, industry, agriculture, free space communication, etc.), rely on good detectors. Conventional quantum detectors were implemented in narrow band-gap semiconductors. However, these materials suffer from fundamental disadvantages and limitations, such as material nonuniformity, relatively high power dissipation, 1/f noise, device passivation. Semiconductor heterostructures of reduced dimensionality are emerging as potential alternatives to bulk narrow-gap materials in implementing optoelectronic devices. Quantum well infrared photodetectors (QWIP's), based on intersubband transitions, represent this trend.<sup>2</sup> In recent years, the study of semiconductor quantum dots (QD) of nanometer size is of particular importance. Charge carriers in such dots are confined in all three dimensions to characteristic lengths which are smaller than their de Broglie wavelengths at working temperatures. In addition to having potential device applications QD's are an excellent stage for experimental studies of basic quantum-mechanical principles. Quantum dot infrared photodetectors (QDIP's) are expected to have two major advantages over QWIP's.<sup>3-8</sup> First, QWIP's have a major drawback that selection rules prohibit the absorption of normal-incident radiation. For intersubband transition to take place, the incident radiation must have an electric field polarized perpendicularly to the layers. Thus one must resort to either wedge illumination, or to implementing gratings over the detector arrays. This limitation can be alleviated in QDIP's as described below.

The second advantage of dots over wells is the potential increase in signal-to-noise ratio. Considering a detector with volume  $V$ , its photocurrent is given by  $I_{\text{opt}} = eG_{\text{opt}}gV$ , and its dark current is  $I_{\text{dark}} = eG_{\text{th}}gV$ , where  $G_{\text{opt}}$  and  $G_{\text{th}}$  are the optical and thermal generation rates, respectively,  $g$  is the gain, and  $e$  is the electronic charge. Assuming that the optical generation rate is uniform throughout the volume, and that generation and recombination are uncorrelated Poissonic processes, the expression for the noise is given by:

$$I_n = \sqrt{4e^2g^2G_{\text{th}}V\Delta f} = \sqrt{4eI_{\text{dark}}g\Delta f}, \quad (1)$$

where  $\Delta f$  is the noise bandwidth. The right-hand square root is the conventional dark noise expression. If, however, we make use of the middle term, we arrive at an expression for the signal-to-noise ratio:

$$\frac{S}{N} = \frac{I_{\text{opt}}}{I_n} = \frac{G_{\text{opt}}\sqrt{V}}{\sqrt{4G_{\text{th}}\Delta f}}. \quad (2)$$

Therefore, increasing the gain,  $g$ , does not affect the signal-to-noise ratio.  $G_{\text{opt}}$  is proportional to the quantum efficiency, and can reach 50–80 % in modern QWIP's by grating techniques. The major drawback of QWIP's as compared to bulk material is the very large thermal generation rate,  $G_{\text{th}}$ , i.e., the very short intraband capture time of excited electrons. [ $G_{\text{th}} = n_0(T)/\tau_c$ , where  $n_0$  is the equilibrium electron concentration above the well, and  $\tau_c$  is the recapture time of excited electrons into the well]. Unlike bulk materials in which a forbidden gap exists between valence and conduction bands, there are no forbidden electron energies between subbands in QW's. The electrons in a QW are confined only

in the growth direction. Thus, there is a continuum of states between the ground level in the well and the barrier in the  $\mathbf{k}_{x,y}$  plane, where  $z$  is the growth direction. Therefore an electron can possess any energy above the first quantized level, and can be captured by the well by emitting a phonon. This strong interaction results in a capture time in the picosecond range. This is about 3–4 orders of magnitude smaller than in intrinsic band-to-band photodetectors, resulting in a low S/N. In QD's the electronic potential is confined in all three dimensions, a zero-dimensional structure is formed, and a totally discrete energy spectrum results.<sup>9</sup> The energy separations between discrete quantized levels in the dot can be designed such that their magnitude will not match the energy of LO phonons or their multiples. Relaxation through acoustic phonons is much weaker since it requires a multiphonon process. One expects suppression of the thermal generation mechanisms of electrons through phonons, and a strong reduction of the noise. Thus the signal-to-noise ratio of QDIP's should be significantly larger than that of QWIP's. This issue is still controversial. Most experimental results that were based on intraband transitions showed increased recombination times in QD's, of the order of 100 ps, compared to  $\sim 2$  ps in QW's.<sup>3,4,10</sup> On the other hand, in a recent paper by Toda *et al.*<sup>11</sup> it is claimed that the 0D density of states is superimposed on a continuum of 2D states. These results suggest an efficient intradot relaxation mechanism, proceeding as follows: The carriers can relax easily within continuum states, and make transitions to the excitonic ground state by resonant emission of localized phonons. The latter conclusion, however, is based on an indirect interpretation of photoluminescence *interband* transitions. Additional studies of intraband transitions in QDIP's are a direct mean to obtain the true recombination mechanisms.

We initiated the use of quantum dots for photodetection using InAs/GaAs material system.<sup>3,4</sup> The work was extended to include more suitable systems, in particular the InAs/InAlAs/InP QD's,<sup>12</sup> in which relatively large dot concentrations are obtained. Moreover, the elongated shape of the dots removes most restrictions imposed by polarization selection rules. Previously reported work on these QDIP's was restricted to 24 K. However, since the intention is to use such devices at much higher temperatures, we report here on experiments performed at 77 K. The high temperature results are compared to the lower ones. New phenomena are reported and interpreted.

## II. InAs/InAlAs/InP QDIPs

### A. Experimental setup

Self-assembled InAs quantum dots were grown using Stranski-Krastanov growth mode in an MBE Riber 2300 reactor.<sup>13</sup> The structure was composed of ten layers of self-assembled InAs dots, separated by 400 Å thick InAlAs barrier layers. The InAlAs was lattice matched to semi-insulating (001) InP substrate. The barriers were delta-doped in their center by Si at a sheet concentration of  $5 \times 10^{11} \text{ cm}^{-2}$ . InGaAs contact layers, 5000 Å thick,  $n$ -doped with Si at a concentration of  $1 \times 10^{18} \text{ cm}^{-3}$  and  $8 \times 10^{18} \text{ cm}^{-3}$ , were grown on the top and the bottom of the

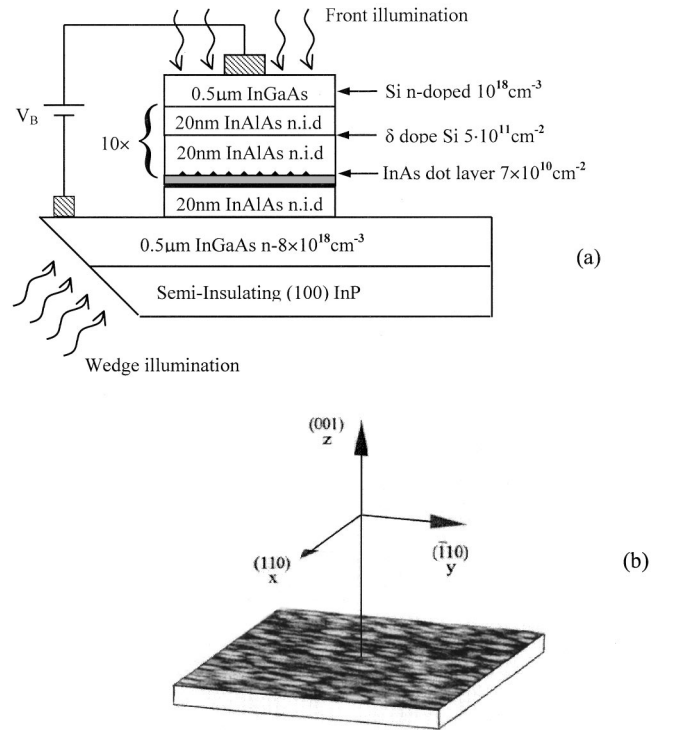


FIG. 1. (a) Detector structure and illumination configurations.  $x$ -polarization is attainable either in front or at wedge illumination. Pure  $y$ -polarization is observed at front illumination, but mixed  $y + z$  polarization at wedge illumination. (b) AFM image of uncapped sample with axes definition.

structure, respectively [see Fig. 1(a)]. The dots grow in a shape of a flattened ellipsoid, around 500 Å long, 300 Å wide, and 20 Å high, with their long axis along the  $[\bar{1}10]$  direction [Fig. 1(b)], and with a high dot concentration of  $7 \times 10^{10} \text{ cm}^{-2}$ .<sup>13</sup>

Since normal-incidence absorption is prohibited in QWIP's, most experimental data are obtained using a wedge [see Fig. 1(a)]. For such configuration the impinging radiation is polarized either parallel to the layers ( $s$ -polarization), or at  $45^\circ$  to the layers ( $p$ -polarization), in which case both perpendicular and parallel polarizations are present. Selection rules for quantum dots allow for absorption of parallel-polarized radiation. Spectra were recorded at normal incidence with polarization either along the  $y$   $[\bar{1}10]$  axis, or along the  $x$   $[110]$  axis. In the wedge configuration, the samples were cleaved along the  $[110]$  and the  $[\bar{1}10]$  directions, and were illuminated through a  $45^\circ$  wedge, polished along the  $[110]$  direction. In the  $s$ -polarization (TE), the electric field is parallel to the width of the dots, the  $x$ -axis. In the  $p$ -polarization, due to the  $45^\circ$  wedge, 50% of the component of the electric field is along the growth  $[001]$  direction (TM),  $z$ -axis, and 50% is in the  $y$  plane. Thus, the observed transitions are polarized both in the  $y$  and  $z$  directions. Here we record spectra for polarization along the height of the dot, which is not attainable in the front illumination. It must be emphasized that, due to the elongated shape of the dots, absorption of radiation polarized along the  $x$ -axis could differ from that at the  $y$ -axis.

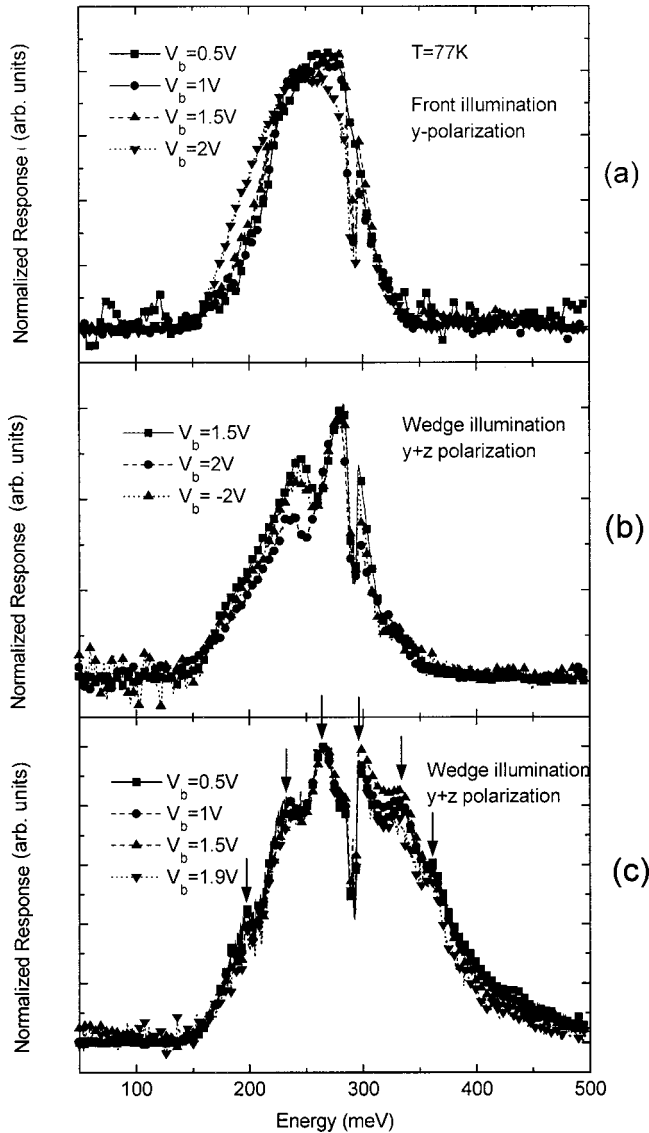


FIG. 2. QDIP photoconductive spectra at 77 K for: (a)  $y$ -axis polarization at front illumination. (b)  $y+z$ -axis polarization at wedge configuration. (c) same as (b) for different detector site and different optical alignment. Note the multipeak nature of the main peak, indicated by arrows. The sharp notch at 290 meV is due to atmospheric  $\text{CO}_2$  absorption.

## B. Experimental results

### 1. Spectral characteristics

The quantum dots were investigated by the photocurrent and absorption spectroscopy. The photoconductive spectra presented here were obtained using a Mattson Cygnus 25 FTIR for various biases and polarizations, at 77 K. Some preliminary experimental results of the same samples at 24 K were reported earlier.<sup>12</sup> Results at both temperatures serve as a basis for the analysis presented here.

Front and wedge illuminated spectra are shown for radiation polarized along the length ( $y$ -axis) [Fig. 2(a)] and the length plus height ( $y+z$ -axis) of the dots [Figs. 2(b) and 2(c)], respectively. The spectra in the figures are normalized by dividing the signal to the bias voltage, and to the amplifier

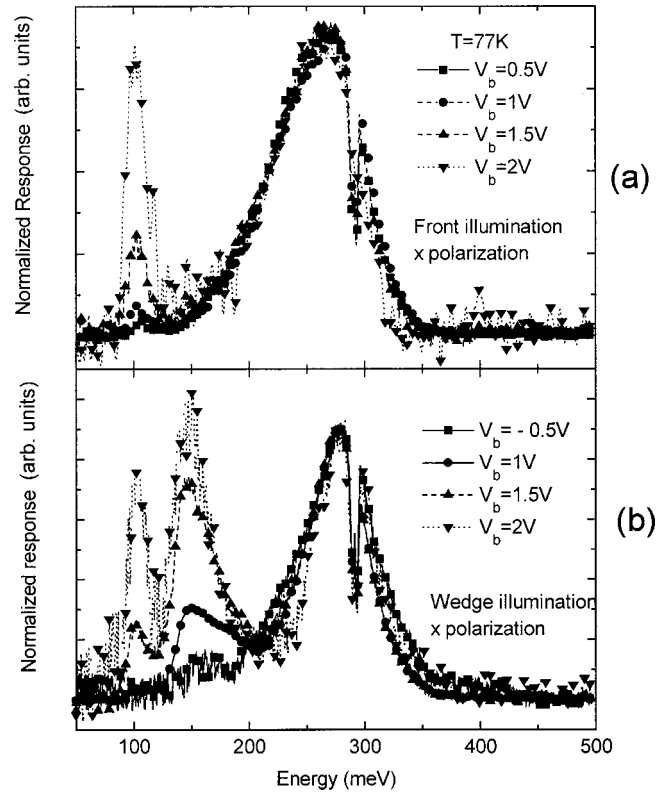


FIG. 3. QDIP spectra at 77 K for  $x$ -axis polarization: (a) front illumination (b) wedge configuration.

gain. At the  $y$  polarization a wide peak, centered at about 260 meV, is observed. The basic waveform for the front,  $y$ -polarized spectra are similar at all biases. However, the structure seems to be composed of more than one peak. The double-peak structure is more pronounced at large biases, where two peaks emerge, at about 240 and 280 meV. (The sharp notch at 290 meV is due to atmospheric  $\text{CO}_2$  absorption). The  $y+z$  polarized spectra obtained with the wedge configuration exhibit a much broader multiple peak. Two examples of such spectra are presented, taken with different detector elements. The first, at Fig. 2(b), is similar to Fig. 2(a), except that the peaks at 240 and 280 meV are well resolved. The second, [Fig. 2(c)] is extending to higher energies, with additional peaks, about 40 meV apart.

New peaks, at about 100 and 150 meV, emerge in the  $x$ -polarized spectra [Figs. 3(a) and 3(b)]. Comparison of the bias dependence of these two peaks to those obtained for the  $y$  spectra shows a striking difference in their behavior. The intensity of the higher-energy band after the spectra are normalized (see above) is unchanged while that of the  $x$ -polarized peaks increases superlinearly. The high-energy band in the  $x$  polarization is narrower, it is not split under all biases, and it is not clear whether the 240 meV component is present at all. Measurements performed in a wedge configuration, presented in Fig. 3(b), show basically the same spectral lines as in the preceding measurements. However, the relative intensities of the various lines are drastically different. In particular, the peak at about 150 meV, which is hardly observed in the front illumination spectrum [Fig. 3(a)] increases with applied bias by orders of magnitude, and at the

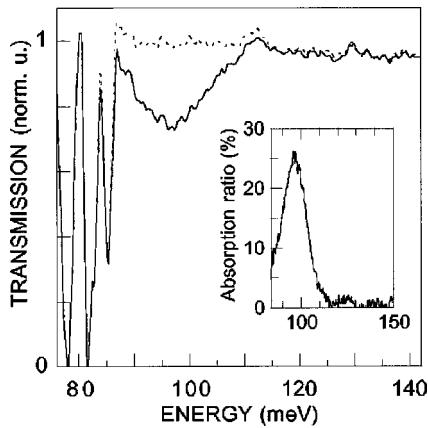


FIG. 4. 77 K normalized transmission spectra at normal incidence of a sample containing ten planes of InAs islands  $n$ -doped at  $1 \times 10^{12} \text{ cm}^{-2}$ . The incident light is polarized parallel to  $[110]$  (full curve) or  $[\bar{1}10]$  (dotted curve). The inset shows the intraband absorption spectrum of the dots for light polarized along  $[110]$ . The spectrum has been obtained by taking the ratio of the  $[110]$  and the  $[\bar{1}10]$  spectra in order to get rid of the InP substrate contribution.

largest bias it becomes the dominant peak.

Infrared absorption measurements were performed on a similar sample but with dot doping concentration of  $1 \times 10^{12} \text{ cm}^{-2}$  and with no contact layers. The normal-incidence spectrum taken at 77 K, is presented in Fig. 4. The unpolarized peaks at 78, 82, and 85 meV are due to two-phonon absorption in the InP substrate. A single,  $x$ -polarized, absorption line appears at about 100 meV. At 77 K this line shows extremely high-peak absorption of about 26% and a full width at half maximum of 15 meV. This peak arises undoubtedly from the same intraband transition as the one reported by Weber *et al.*<sup>14</sup> The oscillator strength is deduced to be  $f = 2m_0\omega\mu^2/\hbar e^2 = 18$ , which is larger than the oscillator strength associated with  $z$ -polarized conduction intersubband transition in GaAs QW's ( $f = 14$ ).

## 2. Detector performance

The detector dark current as a function of bias voltage, presented in Fig. 5, was measured with cold shield to eliminate background radiation for various temperatures in the range of 50–110 K. Also shown is the current due to background radiation for  $F\#1$ , at front illumination, with the detector at  $T = 40$  K. The curves are nonsymmetric with respect to negative and positive bias, as expected from the nonsymmetric structure of the device (i.e., wetting layer exists on one side of the dots, interface roughness different for InAlAs grown on InAs, or vice-versa,  $\delta$ -doping on one side only, etc.). By comparing the background (dotted) curve to the dark current curves, we conclude that background limited infrared performance (BLIP) conditions prevail at 77 K response to all detected energies up to  $\sim 1$ -volt bias. The dominant contribution to the signal up to this voltage is due to the bound-to-continuum broad band at 200–300 meV ( $4\text{--}6 \mu\text{m}$ ). This means that the studied QDIP's are BLIP up to 77 K for this spectral range. This occurs at normal incidence and for detectors with only ten dot periods. There is a sharp increase

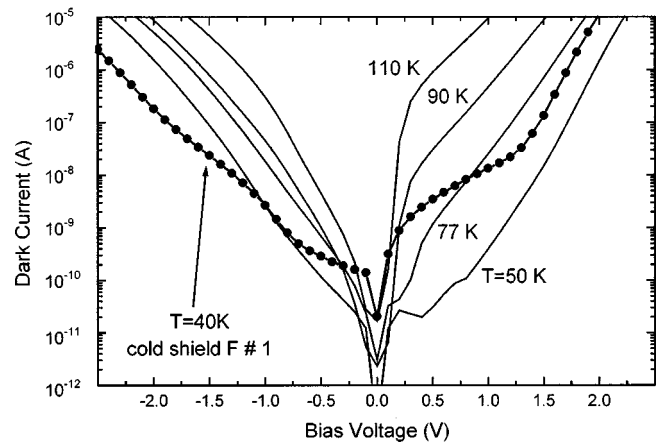


FIG. 5. Dark currents (full lines) and current including 300 K background radiation (dotted curve) characteristics for front illumination. BLIP prevails at 77 K up to a bias of about 0.7 V.

of slope in the dotted  $I$ - $V$  curve of Fig. 5 above 1 V. This coincides with the bias at which the  $8\text{--}12 \mu\text{m}$  peaks start to contribute to the signal. It should be emphasized that BLIP conditions still prevail at these voltages for temperatures up to 60 K.

## C. Analysis and Discussion

Several intriguing features are evident when comparing the various spectra. The responses for normal and wedge excitations polarized in the  $x$  direction should be similar, if not identical. However the measurements of Figs. 3(a) and 3(b) are drastically different. The dominant peak at 150 meV of the spectrum recorded for the wedge configuration is hardly noticeable for front illumination. Similarly, there are major differences between the  $y$  and the  $y+z$ -polarized spectra that cannot be attributed just to the addition of the  $z$ -component. Moreover, the data obtained at 24 K, as reported previously,<sup>12</sup> differs significantly from the present one measured at 77 K.

Four physical mechanisms determine the peak signal intensities in the observed photocurrent:

- Absorption coefficient, which strongly depends on wavelength and dot dimensions.
- Carrier population, which strongly depends on dot dimensions and temperature.
- Effective absorption length—strongly depends on illumination configuration and wavelength.
- Carrier transport to the contacts that result from emission of the confined carriers into the continuum which depends on the excited energy level and the bias.

The difference between the  $y$ -polarized response at the two configurations can most likely be attributed to waveguiding of the incident radiation within the layer. The plasmon-driven index of refraction of the top and bottom InGaAs contact layers is lower than that of the QD structure. Therefore, the wedge-illuminated configuration is confined along the QDIP layers. Obviously, there is no confinement for front illumination. Thus, the effective absorption length is greatly enhanced in the wedge configuration. The multi-

peak character of the high-energy band is attributed to monolayer thickness fluctuations, which vary between three and seven monolayers. Their electron population, the absorption coefficient of the transition, and the effective absorption length affects the contribution of dots of different sizes to the spectra. The larger dots have deeper confined levels. Therefore they are more populated in comparison with smaller dots. On the other hand, the transition energy from the ground state of these dots to the continuum at the barrier is larger. Therefore the absorption coefficient for this transition in larger dots is smaller. The combination of the lower population and larger absorption coefficient will enhance the peak intensity for smaller dots when increasing the absorption length, as evident by comparing the spectra of front and wedge configurations. The relative decrease in population of smaller dots with decreasing temperature causes the broad peak to shift to higher energies at 24 K.<sup>12</sup> A similar broad multipeak was found in photoluminescence (PL) experiments performed on similar structures.<sup>14</sup> This effect is mostly pronounced in Fig. 2(c), in which 6–7 peaks are resolved, with average spacing of about 42 meV. This may be compared to an energy spacing of 58 meV reported by Weber *et al.*<sup>14</sup> The differences arise from including the confinement energy of holes in the interband PL transitions, while those of Fig. 2 are due to pure electronic intraband transitions.

The additional high-energy contribution to the spectra of Fig. 2(c), as compared to Fig. 2(b), stems from the contribution of larger dots, in which the initial energy level is deeper with respect to the barrier level. The absorption coefficient for transitions in the smaller dots is larger than that at the large dots. A short absorption length is enough to saturate the absorption from the small dots, while it is too short for showing the effect for the large ones in front illumination. Increasing the effective absorption length in the wedge configuration enhances the absorption from the bigger dots, which is evident in the spectra. The fact that this effect is more pronounced in Fig. 2(c) than in Fig. 2(b) arises from two possible effects: (a) the spectra were taken for two different detector elements; (b) the illumination conditions were different, causing different coupling of light, thus changing the absorption length in the two experiments.

The wave guiding effect is very sensitive to the radiation wavelength due to the refractive-index dispersion. Thus, the effective absorption length varies with wavelengths. This effect results in the difference between the normal incidence and the wedge illumination for the  $x$ -polarized spectra. It is likely that the enhancement of the peak around 150 meV indicates a strong confinement of radiation at this wavelength, in spite of its low absorption coefficient, as indicated by its absence from the normal-incidence spectra.

Other interesting differences between the spectra at 77 K and those at 24 K (Ref. 12) are the relative intensities of the various peaks. The peak around 320 meV is very strong at all polarizations and configurations at 24 K. At 77 K it appears clearly at the wedge configuration [Fig. 2(c)] and only as a shoulder at other spectra [Figs. 2(a) and 2(b)]. At lower temperatures the larger dots are preferentially occupied with electrons. Although the intraband absorption coefficient is

weaker for the higher-energy transitions, the larger population causes their contribution to dominate the spectrum. As the temperature is increased, the increased population of the smaller dots combined with their larger absorption coefficient shifts the spectra towards lower energies.

The difference between peaks that depend linearly on bias and those which increase superlinearly is a result of the process by which bound electrons turn into free carriers. The various photoconductive peaks can be divided into two groups. The first group is associated with bound-to-bound transitions, followed by tunneling. The intensity of the photocurrent peaks associated with these transitions increases superlinearly with bias since the tunneling probability increases with the barrier bending. The peaks at 100 and 150 meV (12.4 and 8.3  $\mu\text{m}$ ) are identified as such. The first peak increases superlinearly at all biases, while the bias dependence of the second starts superlinear, and turns linear at high biases. This indicates that the excitation of electrons in the 150 meV transition is to a higher bound level than that for the 100 meV peak. The second group of peaks, around 300 meV, increases linearly with bias. This indicates that they are generated by bound-to-continuum transitions.

A simplistic explanation of the observed spectra is suggested. Since the dot structure does not possess any symmetry, all confined energy levels are not degenerated. Thus, each level is populated with up to two electrons. A rough estimate of the number of electrons per dot is given by the ratio of the doping concentration in the barrier to the dot concentration, assuming all free electrons populate the dots. Thus, the number of electrons per dot is about seven. Accordingly, the 3–4 lowest levels are occupied at low temperatures. Since there is a rather large variance in dot size, the upper ones may be full in some dots and empty in others. In the most basic approach it is possible to assume, to a first approximation, that separation of variables applies, and that the dots have the shape of parallelepiped boxes. Therefore, we assign three quantum numbers to each level,  $n_x n_y n_z$ , associated with the  $x$ ,  $y$ , and  $z$  directions. A schematic representation of the confined energy levels in the conduction band of the dots is presented in Fig. 6. The first confined level,  $e1$ , serves as a reference. The figure is based on the parallelepiped dimensions of  $20 \text{ \AA} \times 300 \text{ \AA} \times 500 \text{ \AA}$ . The confinement energy of the ground level depends strongly on the dot size, as stated above. The spacing between the bound levels in individual dots of different sizes is less dependent on the QD dimensions. The allowed transitions are those in which one of the quantum numbers changes by an odd number. Arrows indicate the possible allowed transitions from the populated lower levels. This diagram gives a plausible explanation to the origin of the observed peaks. The arrows also indicate the expected polarization of each transition. The energy level scheme is a modification of the preliminary version of Ref. 12 in view of the results that are presented here. Qualitatively, this scheme resembles the results of Dekel *et al.*<sup>15</sup> which are based on  $\mathbf{k} \cdot \mathbf{p}$  eight-band model.

The single strong peak observed in the absorption spectrum of Fig. 4 is associated with a deep bound-to-bound transition. Two transitions may be assigned tentatively to account for this peak. Those are marked as (a), and (a') in

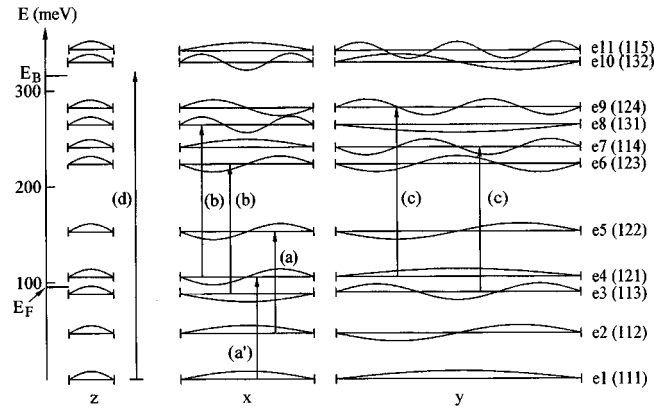


FIG. 6. Simplified schematic representations of the first possible energy levels in the QD, relative to the first confined level. Arrows represent allowed transitions with appropriate polarizations. Only transitions from occupied to unoccupied transitions are indicated. Peaks are polarized in the directions in which the arrows appear.  $E_F$  is the position of the Fermi level,  $E_B$  is the barrier height.

Fig. 6. The peak is strongly polarized along the width of the dots, the  $x$ -axis, as predicted. However, while both transitions may contribute to the absorption, it is reasonable to associate the peak in the photoconductive spectrum mostly with the bound-to-bound  $e2$ - $e5$  transition (a), since tunneling out of the  $e4$  level requires much higher fields than from  $e5$ . As stated above, the peak shows a superlinear dependence on the bias. Its energy is almost unchanged in all samples under all experimental conditions. This agrees with associating it with transitions between deeply-bound states for which their spacing are much less sensitive to dot dimensions. In contrast, the other peaks have slightly different energies for different detector elements, which is interpreted as a difference in average dot sizes along the wafer.

The interpretation of the 150 meV transition is less obvious. It is probably due to more than one transition from a deep to a shallow bound state. It may be associated tentatively with the  $x$ -polarized  $e3$ - $e6$  and  $e4$ - $e8$  transitions [marked by (b)]. Additional symmetry allowed  $y$ -polarized transitions [marked by (c)] are  $e3$ - $e8$  and  $e4$ - $e9$  at 170–180 meV. They do not show up in the spectra, probably due to small associated matrix elements.

All the peaks in the higher-energy broadband are assigned to bound-to-continuum transitions from the ground level, and are represented by a single arrow (d) in Fig. 6. They are basically linearly dependent on the bias, and their polarization selection rules are not as strict, due to the nonsymmetrical shape of the dots. The appearance of the different peaks, and their dependence on experimental configuration are associated with the variation of dot sizes, as described above.

### III. CONCLUSIONS

In conclusion, we presented a detailed photoconductive study of intraband transitions in self-assembled quantum dots. In this high-density matrix we have demonstrated multicolor photoconductive spectra. Either bias voltage or incident radiation polarization controls the dominant peak. In contrast to QWIP's, which prohibits detection at normal incidence, QDIP's allow detection at front illumination, which is comparable in intensity to that of incidence parallel to the layers. A tentative explanation, in terms of a three-dimensional separation of variables, is used. It accounts quite satisfactorily to the identification of the transition energies, polarization selection rules, and the intensities of the observed peaks.

Absorption measurements reveal the oscillator strength of the transition, which depend on the overlap integral between the initial and final levels. These integrals are larger for transitions between two bound levels. The overlap decreases, as the final level becomes shallower. On the other hand, photoconductive measurements depend on both absorption and carrier transport. Thus transitions into shallower levels and into the quasicontinuum are relatively enhanced, and become observable in these measurements.

Thermal generation rate in quantum dots can be significantly smaller than in quantum wells, rendering a much improved signal-to-noise ratio. It is shown here that indeed, BLIP conditions in the detectors presented above prevail at 77 K for integral photocurrent response at  $F\#1$ . The magnitude of detector responsivity at normal incidence is 0.13 A/W, similar to that obtained for polarization normal to the layers, and is comparable to that achieved in QWIP's.

These devices can be implemented to form two-color detector arrays with one common contact, and only one contact for each pixel. This is achieved by alternatively integrating the output at a bias below 1 V to detect the signal that arises from the 3–5  $\mu\text{m}$  range, then at high voltage, to detect both the 3–5 and 10–12  $\mu\text{m}$  range, and subtracting the two. Alternatively, by recording the signal at the same bias at different polarizations. The idea of changing the bias to attain two color detectors was suggested and implemented in QWIP's.<sup>16</sup>

The advantage of the front illumination absorption and the higher signal-to-noise ratio of QDIP's should render a multicolor detector capable of operating at temperatures higher than 77 K. Moreover, the process complexity is reduced since there is no need of multispectral grating for coupling the radiation at different wavelengths, which is a problem that plagues multispectral detection with QWIP's today.

\*Electronic address: finkman@ee.technion.ac.il

<sup>1</sup>W. Herschel, Philos. Trans. R. Soc. London **90**, 284 (1800); *ibid.* **90**, 487 (1800).

<sup>2</sup>B. F. Levine, J. Appl. Phys. **74**, R1 (1993).

<sup>3</sup>E. Finkman, S. Maimon, G. Bahir, S. E. Schacham, and P. M. Petroff, *Intersubband Transitions in Quantum Well: Physics and*

*Devices*, edited by S. S. Li and Y.-K. Su (Kluwer Academic, Boston, 1998) pp. 133–139.

<sup>4</sup>S. Maimon, E. Finkman, G. Bahir, S. E. Schacham, J. M. Garcia, and P. M. Petroff, Appl. Phys. Lett. **73**, 2003 (1998).

<sup>5</sup>D. Pan, E. Towe, and S. Kennerly, Appl. Phys. Lett. **73**, 1937 (1998).

- <sup>6</sup>N. Horiguchi, T. Futatsugi, Y. Nakata, N. Yokoyama, T. Mankad, and P. M. Petroff, *Jpn. J. Appl. Phys., Part 1* **38**, 2559 (1999).
- <sup>7</sup>L. Chu, A. Zrenner, G. Bohm, and G. Abstreiter, *Appl. Phys. Lett.* **75**, 3599 (1999).
- <sup>8</sup>X. Jiang, S. S. Li, and M. Z. Tidrow, *Physica E* **5**, 27 (1999).
- <sup>9</sup>Y. Arakawa and H. Sakaki, *Appl. Phys. Lett.* **40**, 939 (1982).
- <sup>10</sup>S. Kim, M. Erdtmann, and M. Razeghi, *Proc. SPIE* **3629**, 371 (1999).
- <sup>11</sup>Y. Toda, O. Moriwaki, M. Nishioka, and Y. Arakawa, *Phys. Rev. Lett.* **82**, 4114 (1999).
- <sup>12</sup>E. Finkman, S. Maimon, V. Immer, G. Bahir, S. E. Schacham, O. Gauthier-Lafaye, S. Herriot, F. H. Julien, M. Gendry, and J. Brault, *Physica E* **7**, 139 (2000).
- <sup>13</sup>J. Brault, M. Gendry, G. Grenet, G. Holliger, Y. Desieres, and T. Benyatou, *Appl. Phys. Lett.* **73**, 2932 (1998).
- <sup>14</sup>A. Weber, O. Gauthier-Lafaye, F. H. Julien, J. Brault, M. Gendry, Y. Desieres, and T. Benyatou, *Appl. Phys. Lett.* **74**, 413 (1999).
- <sup>15</sup>E. Dekel, D. Gershoni, E. Ehrenfreund, D. Spector, J. M. Garcia, and P. M. Petroff, *Phys. Rev. Lett.* **80**, 4991 (1998).
- <sup>16</sup>E. Martinet, E. Rosencher, F. Luc, Ph. Bois, E. Costard, and S. Delaître, *Appl. Phys. Lett.* **61**, 246 (1992).